Publication Year	2024
Acceptance in OA	2024-07-22T13:52:35Z
Title	Charge-Selective Photocatalytic Degradation of Organic Dyes Driven by Naturally Occurring Halloysite Nanotubes
Authors	Pramanik, Ashim, Calvino, Martina Maria, SCIORTINO, Luisa, Pasbakhsh, Pooria, Cavallaro, Giuseppe, Lazzara, Giuseppe, Messina, Fabrizio, Sciortino, Alice
Publisher's version (DOI)	10.3390/photochem4020009
Handle	http://hdl.handle.net/20.500.12386/35295
Journal	PHOTOCHEM
Volume	4

photochem

MDPI

Article

Charge-Selective Photocatalytic Degradation of Organic Dyes Driven by Naturally Occurring Halloysite Nanotubes

Ashim Pramanik [1], Martina Maria Calvino [1], Luisa Sciortino [2], Pooria Pasbakhsh [3], Giuseppe Cavallaro [1], Giuseppe Lazzara [1], Fabrizio Messina [1] and Alice Sciortino [1,*]

[1] Dipartimento di Fisica e Chimica "Emilio Segrè", Università degli Studi di Palermo, 90123 Palermo, Italy; ashim.pramanik@unipa.it (A.P.); martinamaria.calvino@unipa.it (M.M.C.); giuseppe.cavallaro@unipa.it (G.C.); giuseppe.lazzara@unipa.it (G.L.); fabrizio.messina@unipa.it (F.M.)
[2] Istituto Nazionale di Astrofisica (INAF)/Osservatorio Astronomico di Palermo G.S.Vaiana, Piazza del Parlamento 1, 90134 Palermo, Italy; luisa.sciortino@inaf.it
[3] School of Engineering, Monash University Malaysia, Subang Jaya 47500, Selangor, Malaysia; pooria.pasbakhsh@monash.edu
* Correspondence: alice.sciortino02@unipa.it

Abstract: This study explores the use of Halloysite NanoTubes (HNTs) as photocatalysts capable of decomposing organic dyes under exposure to visible or ultraviolet light. Through a systematic series of photocatalytic experiments, we unveil that the photodegradation of Rhodamine B, used as a model cationic dye, is significantly accelerated in the presence of HNTs. We observe that the extent of RhB photocatalytic degradation in 100 min in the presence of the HNTs is ~four times higher compared to that of bare RhB. Moreover, under optimized conditions, the as-extracted photodegradation rate of RhB (~0.0022 min^{-1}) is comparable to that of the previously reported work on the photodegradation of RhB in the presence of tubular nanostructures. A parallel effect is observed for anionic Coumarin photodegradation, albeit less efficiently. Our analysis attributes this discrepancy to the distinct charge states of the two dyes, influencing their attachment sites on HNTs. Cationic Rhodamine B molecules preferentially attach to the outer surface of HNTs, while anionic Coumarin molecules tend to attach to the inner surface. By leveraging the unique properties of HNTs, a family of naturally occurring nanotube structures, this research offers valuable insights for optimizing photocatalytic systems in the pursuit of effective and eco-friendly solutions for environmental remediation.

Keywords: halloysite nanotubes; natural material; photocatalysis; dyes degradation; charge selectivity

Citation: Pramanik, A.; Calvino, M.M.; Sciortino, L.; Pasbakhsh, P.; Cavallaro, G.; Lazzara, G.; Messina, F.; Sciortino, A. Charge-Selective Photocatalytic Degradation of Organic Dyes Driven by Naturally Occurring Halloysite Nanotubes. *Photochem* **2024**, *4*, 151–162. https://doi.org/10.3390/photochem4020009

Academic Editor: Mirela Petruta Suchea

Received: 18 December 2023
Revised: 18 March 2024
Accepted: 26 March 2024
Published: 28 March 2024

1. Introduction

Environmental contamination by toxic compounds produced by different industrial sectors is a societal issue of key importance, recently aggravated by growing worldwide industrialization and population increase. Organic pollutants and dyes are among the most harmful components spilled into the environment by industrial activities [1–3]. Serious health problems result from the careless spreading of these pollutants into the environment, especially organic molecules with high aqueous solubility. Hence, the need to adopt new and effective strategies to overcome these challenges so as to preserve living ecosystems.

In this regard, nanomaterials can serve the purpose of photocatalysts, activated by sunlight or even by indoor illumination, to achieve the effective degradation of toxic organic waste and thus the refinement of wastewater [4,5]. Photocatalytic decomposition can be driven by nanomaterials through a variety of processes, most importantly the production of reactive oxygen species [6]. Apart from efficiency considerations, several key factors need to be considered when designing photocatalysts. For instance, they should be non-toxic, photostable, cheap, and available. Additionally, the degree of flexibility in the practical application of a photocatalyst also depends on how easily it could be deposited/grown on an inexpensive substrate (glass, cotton, etc.). From the photochemical point of view, the

optical band gap of the photocatalytic material, charge mobility, and surface-to-volume ratio are the most relevant factors controlling their action. Theoretically, when the nanomaterial absorbs photons of a proper wavelength, short enough to overcome the bandgap, the generated photo-electrons and holes move to its outer surface and promote photochemical reactions which are ultimately responsible for photocatalytic function [6–8].

Considering the above-mentioned aspects, various semiconductor nanostructures and nanocomposite materials have become well-known as promising light-harvesting materials for photocatalytic applications, although the actual performance of many of them in real-world applications remains limited. A wide variety of semiconductor nanomaterials such as Titanium dioxide (TiO_2), Silicon dioxide (SiO_2), Bismuth vanadate ($BiVO_4$), ruthenium (Ru)-doped indium oxide (Ru-In_2O_3), Zinc Oxide (ZnO), Cadmium sulphide (CdS), and Tungsten trioxide (WO_3), are being extensively studied for wastewater treatment owing to their meaningful UV light-driven photocatalytic responses [8–12]. However, these photocatalysts are often reported to display toxicity or different forms of chemical instability. For instance, aggregation is a noticeable phenomenon for TiO_2 nanoparticles [13], with detrimental consequences on their photocatalytic performance [14]. Additionally, some of these traditional semiconductor photocatalysts (e.g., $BiVO_4$, Ru-In_2O_3, and WO_3) are not cheap considering their complicated synthesis procedures, and secondary pollution generated during the photocatalytic application of the artificially synthesized metal oxides and sulphides is another concerning side-effect of these emerging technologies [15,16].

A possible strategy that could be used to overcome these challenges is identifying natural earth-abundant minerals which can be directly employed in photocatalytic, photosynthetic, or energy-harvesting applications. The utilisation of green chemistry and clean technology is a fruitful way to synthesize potential photocatalyst which can reduce the amount of secondary pollution. In particular, natural materials may eliminate or substantially reduce the effects of secondary pollution during their photocatalytic applications [4]. Actually, natural minerals having a large surface area and strong adsorption property are also useful as carriers of other photocatalyst materials. Notably, the attachment of a photocatalyst on the surface of natural minerals leads to more surface active sites which can improve the photocatalytic activity [4]. Thus, the efficiency of the photodecomposition of organic pollutants using natural materials as the photocatalyst is reported to be high compared to that of the traditional semiconductor materials [14], and it produces H_2O and CO_2 as non-toxic secondary byproducts. In this respect, halloysite nanotubes (HNTs) are an interesting family of naturally occurring nanomaterials which are chemically related to other natural silicate minerals, and display favourable structural and chemical properties useful for a range of applications [17–19]. In general, HNTs form a hollow tubular-shaped spiral layer of aluminosilicate with the basic unit cell formula of $Al_2Si_2O_5(OH)_4 \cdot nH_2O$ [17]. Importantly, different deposits worldwide offer HNTs with peculiar morphologies, purity, and size distributions [20], and therefore it is considered to be a cheap and abundantly available nanomaterial for a true mass-scale industrial application [21,22]. Compared to other nanotubular particles, such as carbon nanotubes, the world supply of halloysite clay is over 50,000 tons per year [21]. Therefore, as an abundantly available low-cost natural mineral, HNTs may eliminate or substantially reduce the effects of secondary pollution during their photocatalytic applications. Also, HNTs may provide an alternative to expensive carbon nanotubes due to their remarkable chemical stability, structure, high specific surface area, and easy dispersibility [23]. Additionally, HNTs can be used as building blocks for functional composite nanomaterials, assembled via specific and aspecific interactions taking place at their surfaces.

So far, the application of HNTs in photocatalysis has been mostly limited to their use as a substrate for different photocatalysts, or as a performance booster. For example, Mishra et al. [24] have reported on the size- and shape-dependent application of naturally occurring HNTs as a support for TiO_2 nanoparticles as photocatalysts, finding a superior photocatalytic performance in comparison to TiO_2 deposited on a PVC membrane. Another recent study demonstrated the development of a highly efficient photocatalyst comprised

of HNTs-ZnO/GO for the degradation of RhB dye, and 95% photodegradation under UV irradiation was reported [25]. HNTs are also reportedly capable of tuning the optical bandgap of a semiconductor photocatalyst, granting control over the charge recombination process [14].

Interestingly, HNTs can have optical bandgap of ~4 eV, which is more or less similar to a semiconductor photocatalyst such as ZnO [14]. In addition, negative and positive charges exposed at chemically distinct outer and inner HNT surfaces [18] make them capable of charge-selective dye adsorption [26]. Therefore, one may expect HNTs to be inherently capable of photocatalytic activity, at least under UV irradiation, towards some types of organic pollutants, and selectivity may be achieved by using HNTs obtained from different natural resources. So far, HNTs have been used as substrates to enhance the photocatalytic performance of conversional semiconductor photocatalysts e.g., ZnO and TiO_2 nanoparticles [14]. However, focused research on the charge-selective adsorption of organic contaminants over HNT surfaces, and their subsequent photo-degradation under UV irradiation, remains very rare [26].

Photodegradation of cationic RhB and anionic Coumarin 343 (C343) in the presence of unmodified HNTs is reported in this study. A significant acceleration in the photodegradation of RhB is reported, and this effect is attributed to its preferential attachment to the outer surface of HNTs. Notably, the photocatalytic efficiency is also dependent on the inherent chemical composition of HNTs. Under optimized conditions, the as-extracted order of k (~0.0022 min^{-1}) is comparable to that of the previously reported work on photodegradation of RhB in the presence of tubular nanostructures. In contrast, C343 photodegradation occurs less prominently and it is associated with attachment to the inner surface of Halloysites nanotubes. The findings have implications for the development of environmentally friendly and sustainable approaches for wastewater treatment and pollutant remediation, leveraging the unique properties of naturally occurring nanotube structures.

2. Materials and Methods

2.1. Halloysite Nanotubes (HNTs)

HNT samples are naturally occurring, and are similar to those used as light scatterers in our previous research [17]. The halloysite sample obtained from Latah County deposit in NW Idaho, North America, and supplied by I-Minerals Inc (Vancouver, BC, Canada). is named S1 (90% HNTs in weight). The halloysite sample collected from Jarrahdale (Western Australia) from a deeply weathered dolerite profile is named S2. Briefly, the formation of both of these HNTs occurs due to in situ weathering of alumino-silicate minerals. Although, it has a relatively high level (ca. 20%) of other components as well, as confirmed by the X-ray Fluorescence (XRF) measurement given in Ref. [17]. In any case, both of these HNT samples were rinsed with deionized water and dried out under vacuum for 48 h prior to being used in our experiment.

2.2. Characterization of HNTs

The field-emission scanning electron microscopy (FE-SEM, Hitachi SU8010, Tokyo, Japan) technique was used for structural analysis of the HNTs. To this aim, a thin layer of Pt was applied to avoid electrostatic charging. Structural parameters of the HNTs were determined by X-ray diffraction measurement (MiniFlex, Rigaku, Japan). ζ-potential was measured using a ζ-sizer Nano-ZS (Malvern Instruments, Malvern, UK) equipped with a He−Ne laser (λ = 632.8 nm). For ζ-potential experiments, disposable folded capillary cells were used [17]. During the XRD measurement a Cu-Kα radiation source including a nickel filter and working at 40 KV and 15 Ma was used. The wavelength of the X-ray beam was 1.5406 Å and the angle for scanning was ranged from 3° to 70° with a rate of 10° min^{-1} and a step of 0.02°. The optical absorption characteristic of the HNTs was determined from the UV-Vis diffuse reflectance spectrum (DRS) which was measured by the use of an integrating sphere (Labsphere 3PGPS053SL, North Sutton, NH, USA) and a fibre-optic spectrophotometer (Avantes, StarLineULS2048CLEVO, Apeldoorn, The Netherlands). A

125 W Xenon lamp was used as a source of illumination. The functional groups present on the surface of the HNT sample were inspected using Fourier Transformed InfraRed (FTIR) spectroscopic measurement in a FTIR-spectrometer (Spotlight 400, PerkinElmer, Waltham, MA, USA). HNTs dispersed in deionized water were drop casted over a MgF_2 substrate for the FTIR measurement.

2.3. Photocatalytic Experiment

The photocatalytic experiment setup is shown in Figure 1. 1 mL mixture of HNTs (0.1 g/L) with the organic pollutants was poured into a four-sided polished quartz cuvette with a pathlength of 10 mm. The cuvette was then placed over a magnetic stirrer for continuous stirring during the measurement. A 125 W Xenon lamp was used as a source of illumination for the photocatalytic experiment. The light was collected through an optical fibre (THORLABS, 1 mm diameter) and signed over the cuvette as shown in Figure 1. The absorption spectra were measured every 30 s for 1 h using a fibre-optic spectrometer (Avantes, StarLineULS2048CLEVO). We used Rhodamine B (RhB, pKa = 3.2, Sigma Aldrich) and Coumarin 343 (C343, pKa = 4.65, Sigma Aldrich) dye (both having an OD~0.25) as the organic pollutants, and mixed them with distilled water (pH = 7). We performed the photocatalytic experiment with the entire spectral range of the Xenon lamp or blocking the UV part of the excitation source. As part of the real-time measurement, we collected the absorption data during the photocatalytic experiment at a time interval of 1 min and for a total time duration of 120 min. To eliminate the fluctuations of signal due to solid part of the sample, we removed the fluctuating background during data analysis.

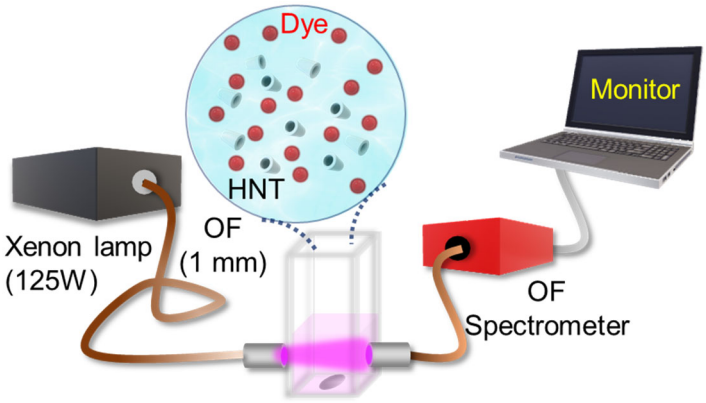

Figure 1. Setup of the photocatalytic experiment.

3. Results and Discussion

3.1. Structural Characterization of the HNTs

The morphology of the two samples of Halloysite Nanotubes (HNTs) was assessed by means of field-emission scanning electron measurements (FESEM), as shown in Figure 2a,b. The images clearly reveal the tubular shape of the HNTs, both the HNTs obtained from North America (hereafter called S1) and the HNTs obtained from Australia (S2). It can also be noticed that the S1 (Figure 2a) nanotubes are larger, with an average lateral size of ~1.8 mm, whereas the average size of the S2 nanotubes is estimated to be ~0.800 mm. Therefore, the S1 sample is expected to have a larger surface area which may help adsorption of organic pollutants. However, the adsorption of organic pollutants over a photocatalyst also depends on surface charge. Therefore, as already reported in our previous work [17], the measured values of the ζ-potential of these HNT samples were found to be $\sim -23.1 \pm 0.4$, and -25.8 ± 0.7 mV, respectively. The general structural and chemical composition of HNT is schematically shown in Figure 2d. A detailed chemical analysis of these samples using XRF has already been presented in our previous work [17]. Notably, in comparison to the S1 sample, the S2 sample contains larger amounts of TiO_2 and Fe_2O_3, which is consistent with the data reported by Pasbakhsh et al. [20]. Here, to verify the chemical identity of our

samples we performed XRD measurements on both HNT samples, the results of which are presented in Figure 2d. The halloysite phase compositions of both of the samples can be identified from the diffraction peaks as indexed in Figure 2c. The positions of the observed diffraction maxima are consistent with earlier reports on HNTs [27–29]. However, the S2 sample may have some quartz (Q) as minor impurities as we have indicted in Figure 2b(ii). In any case, using the Bragg's law the values of the distance d for the S1 and S2 samples were evaluated as ~7.46 and 7.38 Å, respectively. Moreover, we performed FTIR measurements on the HNTs and found that the surface chemical composition is quite similar between the samples. Both spectra show narrow peaks at 3696 cm^{-1} and 3622 cm^{-1} which correspond to the -OH stretching mode in which -OH atoms are inner, i.e., linked to Al atoms [30], a peak at 1120 cm^{-1} which corresponds to the Si-O stretching mode [31], and one at 1638 cm^{-1} which could be due to the presence of interlayer water [32].

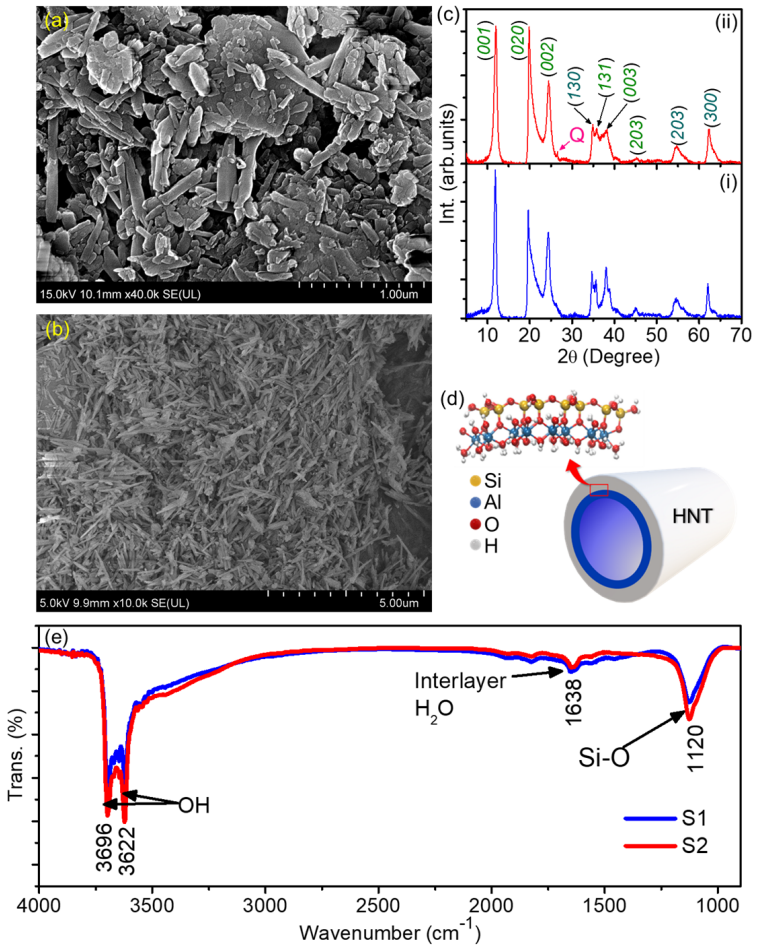

Figure 2. FESEM images of (**a**) S1 and (**b**) S2 sample. (**c**) Schematic of HNT depicting its structure and possible chemical composition. (**d**) XRD profile of (**i**) S1 and (**ii**) S2. The label "Q" in panel (**ii**) indicates minor contribution from quartz impurities. (**e**) FTIR spectra of S1 and S2 samples.

3.2. Photocatalytic Performance of HNTs

We investigated the photocatalytic dye degradation performances of the HNT samples S1 and S2 by suspending them in aqueous solutions of RhB and C343 dye and exposing the resulting mixed colloidal solution to the irradiation of UV-Visible light (125 W Xenon lamp). By increasing the initial concentrations of the pollutants, the degradation rate may be reduced due to their excessive adsorption onto the catalyst surface, hampering the optical absorption property of the catalyst [33]. In addition, the use of an excessive amount of catalyst leads to a decrease in photocatalytic activity due to the scattering of light that prevents the photon from reaching deep into the solution. Also, an excessive catalyst dose

may lead to their self agglomeration and sedimentation which may also be responsible for the decrease in the photocatalytic performance [34,35]. On the other hand, the adsorption properties of HNTs strongly vary at extremely high and low pH values. As has already been reported, the adsorption capacity HNTs for a cationic dye remains unaltered from pH 5 to 7 [32]. Therefore, to determine the ideal experimental conditions, we performed the photocatalytic experiment with different catalysis doses, concentrations of dye, and pH levels, as presented in Figure S1a–c. From the results, the optimised concentration of pollutant, i.e., dyes, catalyst concentrations, and pH value were estimated to be 3 μM, 0.1 g/L, and 7, respectively.

Figure 3 shows the time-dependent absorption spectra of bare RhB dye in the absence and presence of the two types of HNTs, as compared to the effects observed upon irradiation of bare RhB. Even in the absence of HNTs (Figure 3a) the characteristic RhB absorption peak at ~530 nm is observed to gradually decrease with irradiation time, albeit slightly (approximately 10% loss in two hours). This indicates that the RhB is somewhat photobleached even in the absence of any photocatalyst materials; however, a control experiment in the dark (shown in Figure S2) was also performed and it revealed no changes in the absorption spectra within 1 h from the sample preparation. However, the extent of photodegradation can be enhanced in presence of HNTs, as can be seen from Figure 3b,c. In particular, the S2 sample clearly produces a stronger RhB photodegradation as compared to S1 over the same time duration. As a control experiment, we also carried out the photocatalytic experiments for the bare RhB and RhB in the presence of S1 and S2 but blocking the UV portion of the irradiation source (Figure S3a–c), therefore exposing our sample to visible light only. In these conditions, almost no degradation was observed for RhB with any of the combinations of photocatalysts, indicating that the UV component is entirely responsible for the photocatalytic effects observed in Figure 3a–c.

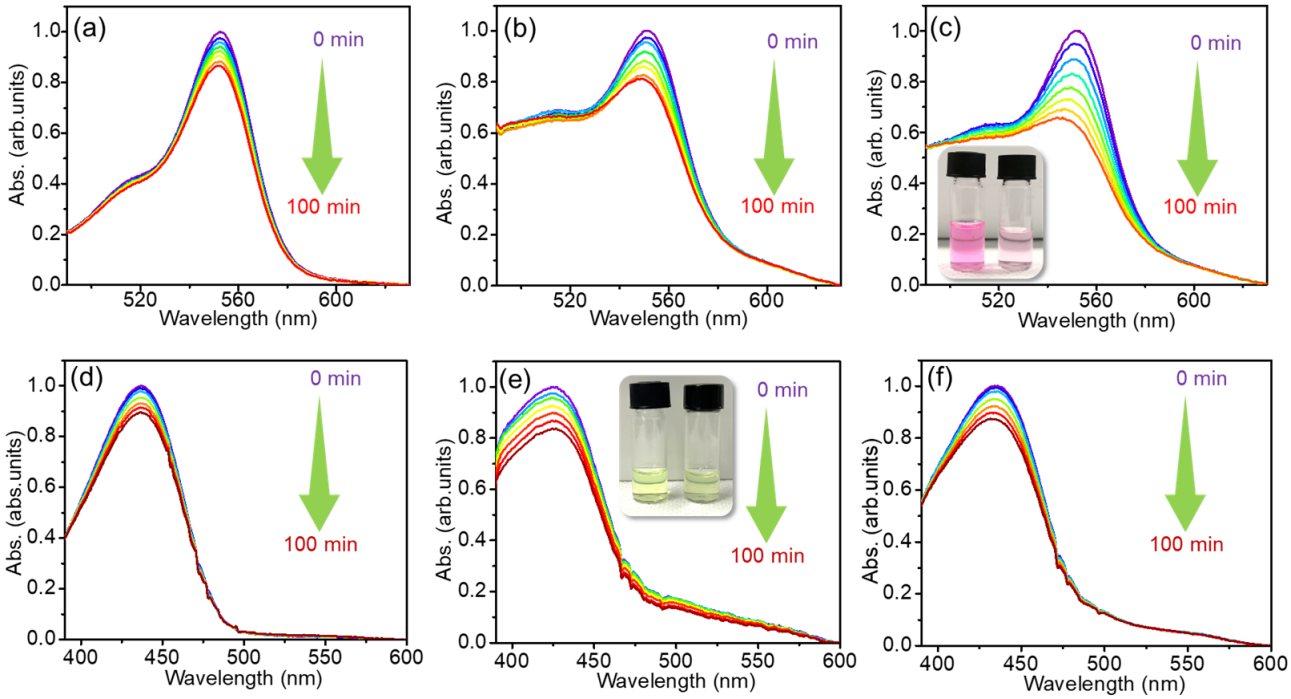

Figure 3. Absorption spectra of (**a**) bare cationic RhB, and RhB in the presence of (**b**) S1 and (**c**) S2 under UV-Visible light irradiation as a function of exposure time; inset of panel (**c**): digital image of RhB dye before and after degradations. Absorption spectra of bare (**d**) anionic C343 dye, and C343 in the presence of (**e**) S1; inset of figure (**e**): digital image of C343 dye before and after degradations, and (**f**) S2 under the UV–Visible light irradiation.

Thereafter, we tested the photodegrading performance of the HNT samples for the C343 dye. Here, we ran two set of experiments, one under UV–Visible light (Figure 3d–f) and one under visible light only (Figure S1d–f). In fact, we found that even the visible component of the lamp is capable of producing a certain degree of photodegradation of C343 (Figure S3d–f), albeit evidently smaller than in the case of RhB. From Figure 3d we can see a less than 10% reduction in the peak absorption of bare C343 after 2 h of UV–Visible light exposure. In contrast, the addition of S1 appreciably enhances the photodegradation effect (Figure 3e). Also, in this case, the addition of S1 enhances the rate of degradation of C343 (Figure 3e), which is now about 20% of C343. In contrast, the photodegradation performance of the S2 (Figure 3f) is smaller than S1, and only slightly larger than that observed for bare C343, both under UV–Visible (Figure 3e,f) and visible (Figure S3d–f) light.

Apart from the photodegradation effects, additional information is contained in Figure 3, including the change in the shape of the absorption spectra. On one hand, the addition of HNTs to the colloidal solutions causes an increase in the absorption coefficient of the order of 0.2 OD throughout the whole region extending from 470 to 600 nm. This can be more easily appreciated from the spectra of the C343 solutions (compare Figure 3d to Figure 3e,f) because C343 displays no absorption in this region. Such an increase in absorption can be promptly attributed to strong light scattering from the large-sized HNTs suspended in water (Figure S4, Supporting Information). However, in the case of RhB we also see an additional change in absorption, of the order of at least 0.4 OD in the region 490–520 nm (compare Figure 3a to Figure 3b,c). As the RhB and C343 experiments were conducted with the same HNT concentrations, these changes cannot be explained as HNT scattering, and must instead be due to a change in the RhB absorption spectra, more precisely a broadening, due to their interactions with the HNTs' surfaces. Thus, at least for RhB, the absorption data provide direct evidence that the photocatalytic effect is driven by the adsorption of the dye onto the surface of the nanotubes, rather than being a collisional effect. Moreover, comparing the spectra recorded at time zero in Figure 3a–c, it is evident that the modification of the shape is simultaneous with the mixing of HNT solution in the dye solution. This suggests that the adsorption of the RhB onto the HNTs is practically instantaneous.

Figure 4 summarises the degradation kinetics of all of the samples, as obtained by extracting the kinetic traces of the evolving absorption from the data in Figure 3. In particular, in Figure 4a,c we report the fractional concentration changes in $\ln(A_0/A)$, as calculated from the absorption measured at the peak. In Figure 4b,d we have reported the quantified values of overall degradation efficiency (η, %) for both of the dyes with time in presence of all samples and in different conditions. The parameter η can be expressed as [2];

$$\eta = [(A_0 - A_t)/A_0] \times 100 \quad (1)$$

where A_0, and A_t are the absorbance of the dye at the beginning of the experiment and at a representative time t = 100 min, respectively. The values of η for both of the dyes in the absence of HNTs are relatively low and are boosted after the addition of HNTs with the dye molecules. We observe that the extent of RhB photocatalytic degradation in 100 min in the presence of S2 is estimated to be ~40%, which is ~4 (~2.3) times higher that of RhB in the absence of HNTs (in presence of S1). Since the natural materials are characterized by diversity, we have conducted a repeatability test to assess the reproducibility of the photocatalytic performance. The values of η under 100 min of UV-Vis light exposure in two tests conducted in identical conditions were found to be in the same range. In regard to C343, under visible irradiation, the degradation efficiency achieved by S1 was found to be ~10%. This is higher than both S2 and the bare dye (Figure 4d), albeit only slightly. This value further increases to ~20% under UV-Vis irradiation, while still remaining lower than the corresponding value recorded for RhB (~40% in presence of S2). The photodegradation efficiency can also be estimated by linear fitting the data under the assumption of pseudo-first order kinetics [36], as is exemplified in Figure S5. From these fittings, we can extract the value of the photocatalytic rate k, which is of the order of 10^{-3} min^{-1}. In fact, the

as-extracted order of k is comparable to that of the previously reported work on the photodegradation of RhB in the presence of HNTs [24] and of different 1-dimensional materials as CNTs [37].

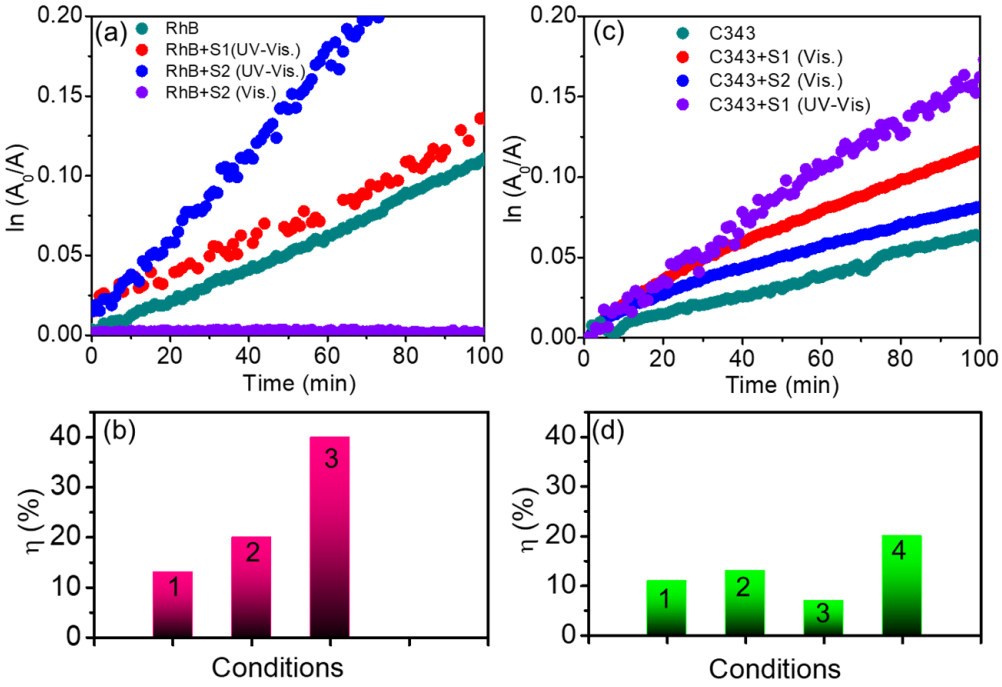

Figure 4. (**a**) Degradation kinetics of cationic RhB dye under different conditions. (**b**) A bar diagram representing the extent of degradation in 100 min (η, %), of the (1) bare RhB and RhB in presence of the S1 (2) and S2 (3) photocatalysts under UV–Visible light irradiation. (**c**) Degradation kinetics of C343 of anionic dye under different conditions. (**d**) A bar diagram representing the extent of degradation (η, %) in 100 min of the (1) bare C343 and C343 in the presence of the S1 (2) or S2 (3) photocatalyst under visible light irradiation and, (4) C343 in presence of S1 under UV–Visible light irradiation.

HNTs are known to be prevalently endowed with a negative charge on their outer surface, due to the presence of Si-OH groups, while their inner surface is positively charged as an effect of Al-OH groups. [18,38]. In fact, their outer negative charge is confirmed by the measured ζ-potential values, which are (-25.8 ± 0.7 mV) and (-23.1 ± 0.4 mV), for S2 and S1, respectively. As pictured in Figure 4, these properties may explain their different photocatalytic performances towards the two dyes, especially when also considering the chemical structure of these molecules. Although RhB is an amphoteric dye containing both positively and negatively charged functional groups, overall, it is cationic in nature [39]. Consequently, it will tend to preferentially interact with the outer surfaces of HNTs. In contrast, one may expect C343 to preferentially interact with HNTs through its negatively charged carbonyl and carboxylic groups, such that it can be expected that C343 is prevalently adsorbed on the inner surface. This could contribute to the smaller photocatalytic effects observed on C343 as compared to RhB, as C343 will be repelled from the outer HNT surfaces, while the inner volume of the nanotubes will be less easily accessible to them. Indeed, a hindered interaction of HNTs with C343, as compared to RhB, is also consistent with the lack of changes in the absorption bandshape of C343 upon the addition of HNTs. In addition to this, we notice that the photodegradation rate (k) of RhB mixed with S2 is higher than the value for S1. We hypothesize that this is related to the traves of TiO_2 and Fe_2O_3 the chemical composition of HNTs [17].

When HNT–dye mixtures are illuminated by UV radiation, their photocatalytic mechanism can be tentatively explained similarly to traditional semiconductor photocatalysts [40], as in Figure 5. The optical band gap of the photocatalysts (HNTs) has been estimated to be ~3.7 eV by diffuse reflectance studies presented in Figure S6 (Supporting Information).

Because HNTs have an optical bandgap of ~3.7 eV, the as-exposed UV irradiation may lead to the photoexcitation of electrons from valence to conduction states (see Figure 5). The activated electron–hole pairs then help to produce reactive oxygen species such as $O_2^{\cdot -}$, and $OH^{\cdot}$ via water reduction and oxidation processes. These reactive oxygen species eventually allow the organic dyes adsorbed on the surface of HNTs to degrade. Considering that HNTs do not significantly absorb in the visible light spectrum, this mechanism cannot be considered responsible for C343 photodegradation under visible illumination. In this case, the initial photon absorption must necessarily occur on the dye, and photodegradation is most likely due to the resulting excited-state charge transfer from the adsorbed dye to the HNTs. In addition, a photodecomposition pathway mediated by water oxidation and reduction is probably hindered for C343 molecules, as they preferentially move inside the HNTs where their interaction with water is severely limited by steric hindrance. Moreover, it is difficult to irradiate the internal part of HNTs. These issues may contribute to the lower efficiency of the photocatalytic processes observed for C343 even under UV light.

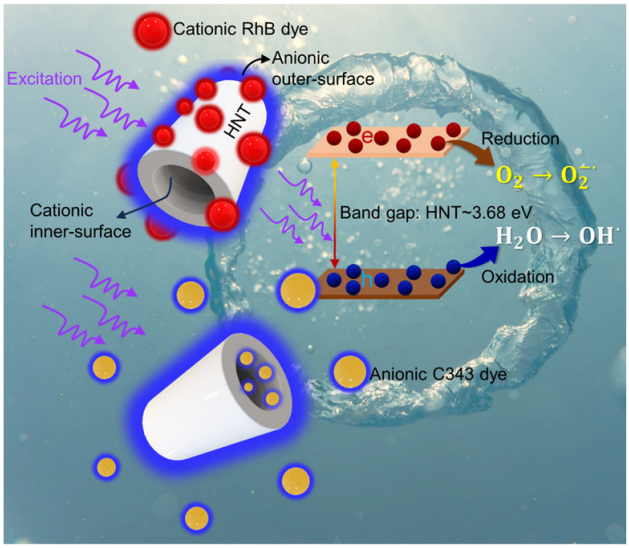

Figure 5. A schematic illustration to explain the degradation mechanism of cationic RhB and anionic C343 dye under UV light irradiation (represented by purple arrows) and in the presence of HNTs.

4. Conclusions

In this study, we investigated the photocatalytic degradation of organic dyes, specifically Rhodamine B and Coumarin 343, promoted by naturally occurring halloysite nanotubes acting as photocatalysts. Through a series of systematic photocatalytic experiments, we demonstrated that the photodegradation of cationic Rhodamine B, which is almost null following the simple exposure of the dye to UV light, is speed up by four times in presence of HNTs. Notably, the photocatalytic efficiency is enhanced when the chemical composition of the HNTs includes TiO_2 and Fe_2O_3. The effect on Coumarin photodegradation is similar to that of Rhodamine B but less efficient. We attribute this behaviour to the different charge states of the two dyes which causes a different attachment site for the dye molecules on the HNTs. Cationic molecules are expected to bind to the outer surface of the HNTs, and on the contrary, anionic molecules should bind to the inner surface of the HNTs, which tends to hinder their photocatalytic action due to steric hindrance issues. The findings presented in this paper have implications for the development of environmentally friendly and sustainable approaches to wastewater treatment and pollutant remediation, leveraging the unique properties of naturally occurring nanotube structures.

Supplementary Materials: The following supporting information can be downloaded at: https://www.mdpi.com/article/10.3390/photochem4020009/s1, Figure S1: Absorption spectra of bare (a) cationic RhB, and RhB in presence of (b) S1 and (c) S2 under the visible light irradiation. Absorption spectra of (d) bare anionic C343 dye and C343 dye in presence of (e) S1 and (f) S2 under visible light irradiation as a function of exposure time; Figure S2: Absorption spectra of (a) C343 and (b) RhB dye in the absence and presence of S2. Simulated: a numerical addition of absorption spectra of bare S2 with dye; Figure S3: Degradation kinetics (fitted with a pseudo-first order linear equation) corresponding to the degradation of (a) cationic RhB dye and (b) anionic C343 dye in presence of S1 and under UV–Visible light irradiation. Figure S4: Absorption spectra of (a) C343, and (b) RhB dye in absence and presence of S2. Simulated: a numerical addition of absorption spectra of bare S2 with dye. Figure S5: Degradation kinetics (fitted with a pseudo-first order linear equation) corresponding to the degradation of (a) cationic RhB dye and (b) anionic C343 dye in presence of S1 and under UV-Visible light irradiation. Figure S6: (a) UV-Vis DRS spectrum of HNTs (0.10 g/L) and (b) the corresponding Tauc plot for HNTs.

Author Contributions: Conceptualization, A.S. and F.M.; Methodology and Analysis, A.P., F.M. and A.S.; Investigation, A.P., M.M.C., L.S. and A.S.; Writing—original draft, A.P., F.M. and A.S.; writing—review and editing, A.P., M.M.C., L.S., P.P., G.C., G.L., F.M. and A.S.; Supervision G.L., F.M. and A.S.; Funding acquisition, A.P., F.M. and A.S. All authors have read and agreed to the published version of the manuscript.

Funding: This research was funded by the Fondo Finalizzato Alla Ricerca Di Ateneo (FFR) 2022–2023 of Unipa; EU financed this research by a Marie Curie Project CARLITO (Grant agreement ID: 101061538).

Data Availability Statement: The data presented in this study are available on request from the corresponding author.

Acknowledgments: The authors thank the LaBAM group for their support and scientific discussions.

Conflicts of Interest: The authors declare no conflicts of interest.

References

1. Carmona-Carmona, A.J.; Mora, E.S.; Flores, J.I.P.; Márquez-Beltrán, C.; Castañeda-Antonio, M.D.; González-Reyna, M.A.; Barrera, M.C.; Misaghian, K.; Lugo, J.E.; Toledo-Solano, M. Photocatalytic Degradation of Methylene Blue by Magnetic Opal/Fe_3O_4 Colloidal Crystals under Visible Light Irradiation. *Photochem* **2023**, *3*, 390–407. [CrossRef]
2. Kumbhakar, P.; Pramanik, A.; Biswas, S.; Kole, A.K.; Sarkar, R.; Kumbhakar, P. In-situ synthesis of rGO-ZnO nanocomposite for demonstration of sunlight driven enhanced photocatalytic and self-cleaning of organic dyes and tea stains of cotton fabrics. *J. Hazard. Mater.* **2018**, *360*, 193–203. [CrossRef] [PubMed]
3. Ren, G.; Han, H.; Wang, Y.; Liu, S.; Zhao, J.; Meng, X.; Li, Z. Recent Advances of Photocatalytic Application in Water Treatment: A Review. *Nanomaterials* **2021**, *11*, 1804. [CrossRef]
4. Tang, X.; Tang, R.; Xiong, S.; Zheng, J.; Li, L.; Zhou, Z.; Gong, D.; Deng, Y.; Su, L.; Liao, C. Application of natural minerals in photocatalytic degradation of organic pollutants: A review. *Sci. Total Environ.* **2022**, *812*, 152434. [CrossRef]
5. Ali, H.M.; Arabpour Roghabadi, F.; Ahmadi, V. Solid-supported photocatalysts for wastewater treatment: Supports contribution in the photocatalysis process. *Sol. Energy* **2023**, *255*, 99–125. [CrossRef]
6. Xiong, L.; Tang, J. Strategies and challenges on selectivity of photocatalytic oxidation of organic substances. *Adv. Energy Mater.* **2021**, *11*, 2003216. [CrossRef]
7. Kumbhakar, P.; Mukherjee, M.; Pramanik, A.; Karmakar, S.; Singh, A.K.; Tiwary, C.S.; Kumbhakar, P. Confinement aided simultanous water cleaning and energy harvesting using atomically thin Wurtzite (Wurtzene). *Adv. Sustain. Syst.* **2021**, *5*, 2000189. [CrossRef]
8. Iang, J.; Shang, J.; Wan, Z. Enhanced Photocatalytic Dehalogenation Performance of RuDoped In_2O_3 Nanoparticles Induced by Oxygen Vacancy. *Photochem* **2023**, *3*, 360–372. [CrossRef]
9. Suhan, M.B.K.; Shuchi, S.B.; Al-Mamun, M.R.; Roy, H.; Islam, M.S. Enhanced UV light-driven photocatalytic degradation of methyl orange using MoO_3/WO_3-fluorinated TiO_2 nanocomposites. *Environ. Nanotechnol. Monit. Manag.* **2022**, *19*, 100768. [CrossRef]
10. Karami, A.; Monsef, R.; Shihan, M.R.; Qassem, L.Y.; Falah, M.W.; Niasari, M.S. UV-light-induced Photocatalytic Response of Pechini Sol–gel Synthesized Erbium Vanadate Nanostructures Toward Degradation of Colored Pollutants. *Environ. Technol. Innov.* **2022**, *28*, 102947. [CrossRef]
11. Dinamani, M.; Surendra, B.S.; Ananda Murthy, H.C.; Basavaraju, N.; Shanbhag, V.V. Green Engineered Synthesis of $Pb_xZn_{1-x}O$ NPs: An Efficient Electrochemical Sensor and UV Light-driven Photocatalytic Applications. *Environ. Nanotechnol. Monit.* **2023**, *20*, 100822. [CrossRef]

12. Chelliah, P.; Gupta, J.K.; Mohammad Wabaidur, S.; Siddiqui, M.R.; Foon Lee, S.; Lai, W.-C. UV-Light-Driven Photocatalytic Dye Degradation and Antibacterial Potentials of Biosynthesized SiO_2 Nanoparticles. *Water* **2023**, *15*, 2973. [CrossRef]
13. Chen, D.; Cheng, Y.; Zhou, N.; Chen, P.; Wang, Y.; Li, K.; Huo, S.; Cheng, P.; Peng, P.; Zhang, R.; et al. Photocatalytic degradation of organic pollutants using TiO_2-based photocatalysts: A review. *J. Clean. Prod.* **2020**, *268*, 121725. [CrossRef]
14. Peng, H.; Liu, X.; Tang, W.; Ma, R. Facile Synthesis and Characterization of ZnO Nanoparticles Grown on Halloysite Nanotubes for Enhanced Photocatalytic Properties. *Sci. Rep.* **2017**, *7*, 2250. [CrossRef] [PubMed]
15. Jia, Z.; Li, T.; Zheng, Z.; Zhang, J.; Liu, J.; Li, R.; Wang, Y.; Zhang, X.; Wang, Y.; Fan, C. The BiOCl/diatomite Composites for Rapid Photocatalytic Degradation of Ciprofloxacin: Efficiency, Toxicity Evaluation, Mechanisms and Pathways. *Chem. Eng. J.* **2020**, *380*, 122422. [CrossRef]
16. Hu, X.; Sun, Z.; Song, J.; Zhang, G.; Li, C.; Zheng, S. Synthesis of Novel Ternary Heterogeneous BiOCl/TiO_2/sepiolite Composite with Enhanced Visible-light-induced Photocatalytic Activity Towards Tetracycline. *J. Colloid Interface Sci.* **2019**, *533*, 238–250. [CrossRef] [PubMed]
17. Pramanik, A.; Sciortino, A.; Reale, M.; Pasbakhsh, P.; Cavallaro, G.; Cannas, M.; Lazzara, G.; Messina, F. Naturally Occurring Halloysite Nanotubes as Light Scatterers for Stable Random Lasing Applications. *ACS Appl. Nano Mater.* **2023**, *6*, 15896–15905. [CrossRef]
18. Massaro, M.; Lazzara, G.; Milioto, S.; Noto, R.; Riela, S. Covalently Modified Halloysite Clay Nanotubes: Synthesis, Properties, Biological and Medical Applications. *J. Mater. Chem. B* **2017**, *5*, 2867–2882. [CrossRef]
19. Yuan, P.; Tan, D.; Annabi-Bergaya, F. Properties and Applications of Halloysite Nanotubes: Recent Research Advances and Future Prospects. *Appl. Clay Sci.* **2015**, *112–113*, 75–93. [CrossRef]
20. Pasbakhsh, P.; Churchman, G.J.; Keeling, J.L. Characterisation of Properties of Various Halloysites Relevant to their Use as Nanotubes and Microfibre Fillers. *Appl. Clay Sci.* **2013**, *74*, 47–57. [CrossRef]
21. Abdullayev, E.; Lvov, Y. Halloysite clay nanotubes for controlled release of protective agents. *J. Nanosci. Nanotechnol.* **2011**, *11*, 10007–10026. [CrossRef] [PubMed]
22. Fahimizadeh, M.; Wong, L.W.; Baifa, Z.; Sadjadi, S.; Auckloo, S.A.B.; Palaniandy, K.; Pasbakhsh, P.; Tan, J.B.L.; Singh, R.R.; Yuan, P. Halloysite clay nanotubes: Innovative applications by smart systems. *Appl. Clay Sci.* **2024**, *251*, 107319. [CrossRef]
23. Zubkiewicz, A.; Szymczyk, A.; Franciszczak, P.; Kochmanska, A.; Janowska, I.; Paszkiewicz, S. Comparing Multi-Walled Carbon Nanotubes and Halloysite Nanotubes as Reinforcements in EVA Nanocomposites. *Materials* **2020**, *13*, 3809. [CrossRef] [PubMed]
24. Mishra, G.; Mukhopadhyay, M. TiO_2 Decorated Functionalized Halloysite Nanotubes (TiO_2@ HNTs) and Photocatalytic PVC Membranes Synthesis, Characterization and its Application in Water Treatment. *Sci. Rep.* **2019**, *9*, 4345. [CrossRef] [PubMed]
25. Park, J.; Lee, H.; Lee, K.; Noh, S.; Jin, S.; Jae, J.; Jeong, Y.; Noh, J. ZnO/Graphene Oxide on Halloysite Nanotubes as a Superabsorbent Nanocomposite Photocatalyst for the Degradation of Organic Dyes. *Nanomaterials* **2023**, *13*, 1895. [CrossRef] [PubMed]
26. Kanani-Jazi, M.H.; Akbari, S. Amino-Dendritic and Carboxyl Functionalized Halloysite Nanotubes for Highly Efficient Removal of Cationic and Anionic Dyes: Kinetic, Isotherm, and Thermodynamic Studies. *J. Environ. Chem. Eng.* **2021**, *9*, 105214. [CrossRef]
27. Jiang, D.; Jing, H.; Liu, Z.; Jia, C.; Liu, Q. Natural Halloysite Nanotube as a Spatially Confined Nanoreactor for Improving Photocatalytic Performance. *J. Phys. Chem. C* **2021**, *125*, 15316–15323. [CrossRef]
28. Wang, X.; Guo, H.; Wang, F.; Tan, T.; Wu, H.; Zhang, H. Halloysite Nanotubes: An Eco-friendly Adsorbent for the Adsorption of Th(IV)/U(VI) Ions from Aqueous Solution. *J. Radioanal. Nucl. Chem.* **2020**, *324*, 1151–1165. [CrossRef]
29. Sun, P.; Liu, G.; Lv, D.; Dong, X.; Wu, J.; Wang, D. Effective Activation of Halloysite Nanotubes by Piranha Solution for Amine Modification via Silane Coupling Chemistry. *RSC Adv.* **2015**, *5*, 52916–52925. [CrossRef]
30. Wu, Y.; Yang, Y.; Liu, H.; Yao, X.; Leng, F.; Chen, Y.; Tian, W. Long-term Aantibacterial Protected Cotton Fabric Coating by Controlled Release of Chlorhexidine Gluconate from Halloysite Nanotubes. *RSC Adv.* **2017**, *7*, 18917–18925. [CrossRef]
31. Zhang, Y.; He, X.; Ouyang, J.; Yang, H. Palladium Nanoparticles Deposited on Silanized Halloysite Nanotubes: Synthesis, Characterization and Enhanced Catalytic Property. *Sci. Rep.* **2013**, *3*, 2948. [CrossRef] [PubMed]
32. Luo, P.; Zhao, Y.; Zhang, B.; Liu, J.; Yang, Y.; Liu, J. Study on the Adsorption of Neutral Red from Aqueous Solution onto Halloysite Nanotubes. *Water Res.* **2010**, *44*, 1489–1497. [CrossRef] [PubMed]
33. Zhang, D.; Lv, S.; Luo, Z. A study on the photocatalytic degradation performance of a $[KNbO_3]_{0.9}$-$[BaNi_{0.5}Nb_{0.5}O_{3-\delta}]_{0.1}$ perovskite. *RSC Adv.* **2020**, *10*, 1275–1280. [CrossRef] [PubMed]
34. Kashif, N.; Ouyang, F. Parameters Effect on Heterogeneous Photocatalysed Degradation of Phenol in Aqueous Dispersion of TiO_2. *J. Environ. Sci.* **2009**, *21*, 527–533. [CrossRef] [PubMed]
35. Mittal, A.; Sharma, S.; Kumari, V.; Yadav, S.; Chauhan, N.S.; Kumar, N. Highly efficient, visible active TiO_2/CdS/ZnS photocatalyst, study of activity in an ultra low energy consumption LED based photo reactor. *J. Mater. Sci. Mater. Electron.* **2009**, *30*, 17933–17946. [CrossRef]
36. Karmakar, S.; Pramanik, A.; Kole, A.K.; Chatterjee, U.; Kumbhakar, P. Syntheses of Flower and Tube-like $MoSe_2$ Nanostructures for Ultrafast Piezocatalytic Degradation of Organic Dyes on Cotton Fabrics. *J. Hazard. Mater.* **2022**, *424*, 127702. [CrossRef]
37. Udrescu, A.; Florica, S.; Chivu, M.; Mercioniu, I.; Matei, E.; Baibarac, M. Rhodamine B Photodegradation in Aqueous Solutions Containing Nitrogen Doped TiO_2 and Carbon Nanotubes Composites. *Molecules* **2021**, *26*, 7237. [CrossRef] [PubMed]
38. Bretti, C.; Cataldo, S.; Gianguzza, A.; Lando, G.; Lazzara, G.; Pettignano, A.; Sammartano, S. Thermodynamics of Proton Binding of Halloysite Nanotubes. *J. Phys. Chem. C* **2016**, *120*, 7849–7859. [CrossRef]

39. Nguyen, K.M.V.; Phan, A.V.N.; Dang, N.T.; Tran, T.Q.; Duong, H.K.; Nguyen, H.N.; Nguyen, M.V. Efficiently Improving the Adsorption Capacity of the Rhodamine B Dye in a SO_3H-functionalized Chromium-based Metal–organic Framework. *Mater. Adv.* **2023**, *4*, 2636–2647. [CrossRef]
40. Abid, M.; Ben Haj Amara, A.; Bechelany, M. Halloysite-TiO_2 Nanocomposites for Water Treatment: A Review. *Nanomaterials* **2023**, *13*, 1578. [CrossRef]